Optics Communications 480 (2021) 126494

Contents lists available at ScienceDirect

Optics Communications

journal homepage: www.elsevier.com/locate/optcom

Advanced visualization using image super-resolution method for three-dimensional mobile system

Munkh-Uchral Erdenebat [a], Yan-Ling Piao [a], Ki-Chul Kwon [a], Moung Hee Lee [a], Ki Hoon Kwon [b], Min Young Kim [b], Nam Kim [a,*]

[a] School of Information and Communications Engineering, Chungbuk National University, 1 Chungdae-ro, Seowon-gu, Cheongju, Chungbuk 28644, South Korea
[b] School of Electronics Engineering, Kyungpook National University, 80 Daehak-ro, Buk-gu, Daegu 41566, South Korea

ARTICLE INFO

Keywords:
3D mobile system
Computer-generated integral imaging
Advanced visualization method

ABSTRACT

A three-dimensional mobile system with advanced visualization based on image super-resolution method is proposed and implemented. Here, real object information is acquired using three-dimensional scanning, and the three-dimensional visualizations of the object with the improved resolution are displayed on the mobile display with user interaction functionality. Unlike the previous methods, an advanced visualization method displays the resolution-enhanced reconstructed images without the degradation of the quality. From the experimental results, the proposed system presented clearer visualizations of the object, and the quantitative evaluation methods confirm that the proposed system provides the higher-resolution visualizations of the real object without loss of quality on the mobile display.

1. Introduction

In recent years, three-dimensional (3D) imaging systems have been attracted interest because they can meet the demands of modern customers and the needs of future technologies [1,2]. Specifically, following the development of communication technologies, 3D imaging systems are being developed for mobile environments. Integral imaging is a 3D imaging technique that acquires an object's 3D data using a two-dimensional (2D) lens array in a single exposure, and can display a natural full-parallax, full-color and continuous-viewing 3D visualization [2–4]. Unlike 3D display technologies such as stereoscopic and holographic systems [5,6], integral imaging technique picks up 3D information about the object using incoherent light via a simple process. However, the elemental image array (EIA) which is a 2D image including the 3D information of the object, is captured in low-quality form through the lens array, due to several optical issues such as distortion and contamination of lens array. Accordingly, the 3D images are reconstructed in a low-quality form. The computer-generated integral imaging method provides a solution for these issues, by generating the EIA virtually through computer graphics. In this way, the EIA is generated perfectly using the virtual lens array, and the quality of the reconstructed 3D image is improved [7,8]. However, EIAs using computer-generated integral imaging are only generated for virtual objects that do not exist in the real world.

A simplified integral imaging pickup method, proposed by G. Li et al. demonstrated the functionality of a computer-generated integral imaging algorithm that can acquire full 3D information for real objects [9]. Here, the depth and color information of a real object is taken by using a depth camera, and the EIA is generated through computer-generated integral imaging. The 3D image is reconstructed optically using the lens array. Thereafter, based on an image space parallel processing algorithm using a graphics processing unit (GPU) [10–12], the simplified integral imaging pickup method was upgraded to a real-time display by J.-S. Jeong et al. [13]. However, these methods can only be conducted using PC-based processing and are therefore impractical for daily use.

M.-U. Erdenebat et al. proposed a 3D mobile system based on integral imaging that the 3D information of a real object is acquired by the depth camera and the 3D visualizations of a real object is presented on a mobile device's display [14]. Although the system demonstrated the potential of this kind of approach, the images were reconstructed with insufficient resolution and quality. Basically, the resolution of directional sub-images of an orthographic-view image is improved by increasing the number of elemental images, because the number of elemental images is identical to the number of pixels in directional-view images. An interpolation-based method was recently used for a 3D mobile system [15]. Here, additional intermediate-view elemental images were generated between each neighboring elemental image, and the number of elemental images was varied based on how many times the intermediate-view elemental images were generated; thus, the resolution of the reconstructed images could be increased. However,

* Corresponding author.
E-mail address: namkim@chungbuk.ac.kr (N. Kim).

https://doi.org/10.1016/j.optcom.2020.126494
Received 11 June 2020; Received in revised form 23 September 2020; Accepted 27 September 2020
Available online 29 September 2020

the quality of the reconstructed images was decreased following the generation of each additional intermediate-view elemental image. Furthermore, the intermediate-view elemental images increase the size of the EIA too much, and digital reconstruction requires a large memory capacity and a long computation time [16]. It is difficult to apply arbitrary methods in a mobile environment, unlike general integral imaging methods.

Recently, the image super-resolution (SR) algorithms that convert the low-resolution images into the high-resolution image through the deep learning, also known as convolutional neural network (CNN), have been suggested [17–22]. In the case of traditional SR methods that do not apply CNN, several algorithms that proceed each processing step are collectively combined to create a high-resolution image. Unlike the traditional methods, CNN-based SR algorithms are end-to-end methods that proceed with all steps in a single integrated model and show higher performance compared to the traditional SR methods (without CNN). Also, it has been verified that the SR methods can be effective for light field displays [23–25]. Although these methods showed good results through the SR algorithms, it is difficult to directly use the same algorithms in the proposed system; because it should be suitable for the configuration and data type.

So, in this study, a 3D mobile display with an advanced visualization using a deep learning-based SR algorithm is proposed. Here, as the SR algorithm is integrated with the digital reconstructions, and it is possible to solve the problem that improving the resolution of reconstructed images while the quality is guaranteed. In addition, a 3D scanning method is used for data acquisition [26]. Real 3D object data are acquired with high accuracy and resolution, and the SR model-based visualization method can display the resolution-enhanced reconstructed images with no loss of quality. This method was validated experimentally.

2. Proposed method

As shown in Fig. 1, the main procedures of the proposed system are as follows: the 3D scanner collects the 3D data of a real object; the acquired data are transmitted to the mobile device and normalized; the EIA is generated from the normalized data using a virtual lens array with input parameters; 3D visualizations of the object, orthographic-view image, and depth-slices, are reconstructed through the advanced visualization method and displayed on the mobile device with the user interaction function.

The 3D scanner acquires more accurate 3D information from the real-world object, instead of simply capturing depth and red-green-blue (RGB) images via a fixed depth camera; therefore, it provides an opportunity to improve the quality of the final displayed image. The acquired 3D object data are transmitted to the mobile device and stored as a virtual 3D model that comprises a matrix (x, y, z, R, G, B) containing the coordinate and color information of each object point or vertex of the 3D model. Note that only the external information of the object is acquired; therefore, no additional algorithms for occlusion removal, such as hidden point removal operators [27,28], are required in subsequent processing. Although the 3D scanning method provides clearer images than a conventional fixed-depth camera-based method, the resolution of reconstructed images should be improved for comfortable viewing.

When the acquired 3D data are transmitted to the mobile device, the data is pre-processed in preparation for EIA generation. Here, the depth information should be normalized for the depth-of-field of the lens array such that a 3D image can be visualized appropriately. The depth information of each object point can be normalized as:

$$z' = \frac{2z \times z_{CDP}}{z_{\max} + z_{\min}}, \tag{1}$$

where z_{CDP} is the distance between the central depth plane of the 3D model and the virtual lens array that can be calculated using the Gaussian lens law, and $z_{\max}$ and $z_{\min}$ are the maximum and minimum values of the original depth information. If the original depth information is not normalized, object points with very high z values are imaged at orthogonal planes outside the boundaries of the depth-of-field of the lens array; hence, such points are reconstructed as defocused and/or blurred. Once the depth information has been normalized, the center of the width and height of the virtual 3D model is set to 0, and the center of the depth is set to z_{CDP}.

Based on the depth-normalized 3D model, the virtual lens array, and the EIA plane, the EIA generation environment is configured. Even though the optical reconstruction method is excluded from the proposed system, the EIA must be generated as non-overlapped (the size of each elemental image is identical to pitch of each elemental lens) in order to reconstruct the 3D images of an object through the integral imaging-based visualization method properly. The specifications of the virtual lens array and other parameters of the EIA generation, such as the pitch, focal length and number of the elemental lenses, the gap between the lens array and the EIA plane, and the pixel size of the EIA plane are inputted by the user. The resolution of the EIA plane is defined by the number and size of elemental lenses, and by the display pixel pitch, as follows:

$$EIA\left(EI_X, EI_Y\right) = \left(\frac{N_X \times P_{EL}}{P_D}, \frac{N_Y \times P_{EL}}{P_D}\right), \tag{2}$$

where EI_X and EI_Y are the sizes of an EIA along the X and Y axes, respectively, N_X and N_Y are the number of elemental lenses and/or elemental images along the X and Y axes, respectively, P_{EL} is pitch of the elemental lens, and P_D is the pixel size of the EIA plane, which is same as the pixel pitch of the mobile display. During the EIA generation process, each pixel of the EIA is imaged from the depth-normalized 3D model through the virtual lens array, and corresponding color information is covered when the object point is imaged onto the EIA plane. However, for the object points that cannot be imaged as pixels in the EIA plane, color information cannot be determined, so these pixels are visualized as black. Note that, since the point cloud model contains the full 3D information of the object, it seems that displaying the normalized point cloud model directly as it is on a mobile display can be an effective way to represent the 3D visualization of the object. However, the displaying process becomes complicated when the point cloud model is displayed as it is. Also, the external appearance and shape of the object can be observed, but it is difficult to view 3D information such as parallax and depth. And in order to observe this 3D information, the user interaction functions such as rotation and zoom-in/zoom-out are required; however, it is difficult to process these functions in a mobile environment due to low performance, especially when the number of object points is large. Therefore, the computer-generated integral imaging and digital reconstruction methods based on non-overlapped EIAs are used in this system to display the 3D visualization of a normalized point cloud model.

After the EIA is generated, an advanced (SR-based) visualization method reconstructs the resolution-enhanced 3D visualizations of objects with no loss of quality and displays them on the mobile device. Fig. 2 shows a schematic diagram of the EIA to visualization. In the visualization, first, the orthographic-view image and depth-slices of the object are reconstructed initially, but are not displayed directly; rather, each is stored individually for further processing. Note that the orthographic-view image indicates the parallax information of the object, and depth slices indicate the depth information. Then, the CNN model improves the resolution and filters the noise of all reconstructed images through the convolutional layers. Finally, the resolution-enhanced reconstructed output images of the SR model are displayed on the mobile device. Unlike the conventional system, the lens array is not utilized in the display part of proposed system, and the application of the proposed visualization method allows the touchscreen as a user interface.

The resolution of the image is enhanced according to the selected factor. Note that the resolution of the input images can be improved n

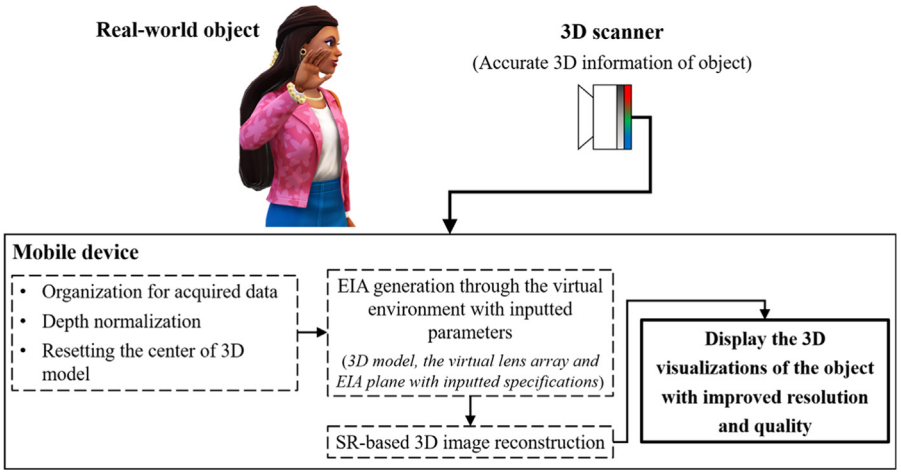

Fig. 1. Scheme of the main procedures of a proposed 3D mobile system with SR-based visualization method.

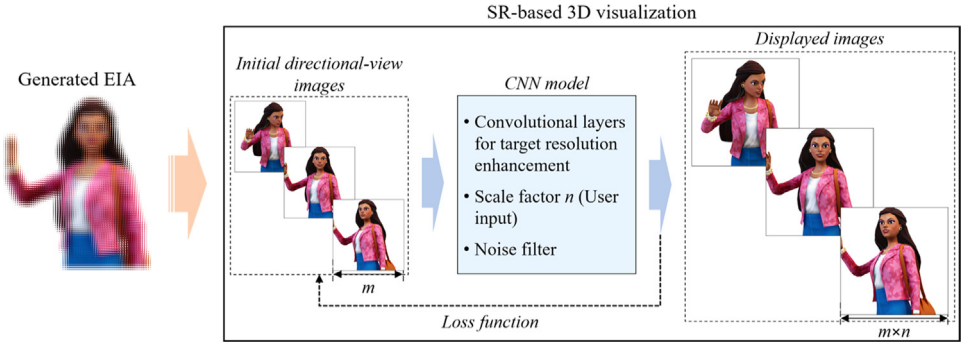

Fig. 2. Schematic diagram of the pre-trained SR model for resolution-enhancement and noise-filtering from the input initially reconstructed images.

times in each direction. The reconstruction and display process through the SR-based visualization method is as follows: the initially generated directional-view images are inputted into the CNN model and the target resolution enhancement is calculated according to the scale factor. Then, the loss function is derived from a comparison of the input image properties and the target image. Finally, the CNN learning model receives the error values and optimizes the parameters of the image through layers of the model. These processes are iterated until the output image is matched most closely to the corresponding input image, while the image noise filtering process is performed simultaneously. Note that the proposed system acquires the real-world object data with limited resolution, and it is difficult to show good results for some SR algorithms. Therefore, the purpose of the proposed system is to apply the most suitable SR algorithm into the 3D mobile system for advanced 3D image visualization, instead of focusing on a single SR algorithm. Since the proposed system is a network-based system; therefore, the SR algorithm should be uncomplicated (consisting of very many convolutional layers, etc.), the image processing speed is as fast as possible, and GPU processing, etc., should be excluded. So, we tested the proposed method with several SR algorithms, and the experimental results obtained through the most efficient method are presented in the next section. Also, the proposed system expresses 3D information of a real object on a 2D mobile display through the lens array-free advanced visualization method, and the SR algorithm does not have the function like shifting the pixels or estimating the disparity in each perspective; therefore, the spatial-angular redundancies do not occur, and the related analysis is not required [2,29,30].

It is impossible to complete all processes of the proposed system within the mobile environment due to the limited performance. Therefore, the data organization, EIA generation, and SR algorithm-based visualization processes use network-based processing, such as cloud computing. In other words, the processes mentioned above proceed via cloud computing after the original data are uploaded; and the final reconstructed images are transmitted back from the cloud to a mobile device and displayed on the mobile display. Note that conventional methods generate the EIA in the mobile environment for optical reconstruction, whereas in the proposed system, optical reconstruction is not required such that the EIA does not need to be generated by the mobile device. It is expected that 5G mobile network (10 Gbps upload/20 Gbps download speeds, 1 ms delay time and mmWave wide bandwidth) [31] which is now becoming available to the public, will provide great opportunities for real application and the day-to-day basis of the proposed system. This high degree of specifications is particularly helpful for the rapid transmission of large amounts of data for the proposed system.

3. Experimental results

Fig. 3 shows the experimental setup of the proposed system including a 3D scanner for real object (Fig. 3(a)) and the user interface of a host program on a mobile device (Fig. 3(b)). In the experiment, an 8.4″ Dell Venue 8-7840 tablet with an Intel Z3580 quad-core 2.33 GHz central processing unit, 2 GB memory and resolution of 2560×1600 pixels (pixel pitch: 0.07056 mm) was used. Note that the proposed system also can be operated on smartphones, because the same operating is installed on the tablet and smartphone, and the operation method is also the same. But the experiment was conducted on a tablet with high pixel density and large screen, in order to check the displayed image in detail. As mentioned above, cloud computing is required for the proposed system; however, in the experiment, due to the lack of real cloud computing server and 5G environment, a PC server (without using a GPU processing) with the same function to cloud computing

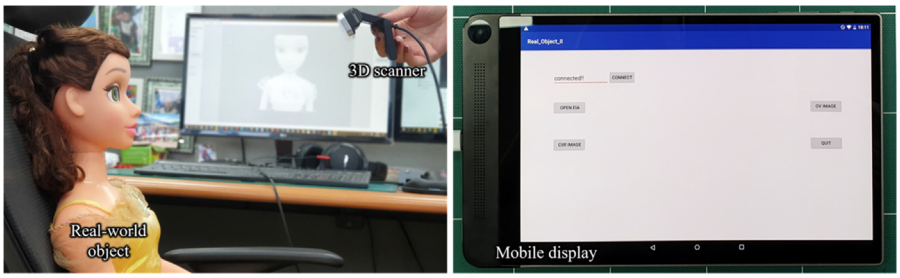

Fig. 3. Experimental configuration of the proposed system: (a) a 3D scanner for real object and (b) a user interface on mobile device.

was used and connected to the mobile device via an 802.11n wireless connection with 2.4 GHz frequency which has 150 Mbps theoretical speed (50–60 Mbps actual speed during the experiment).

3.1. Data acquisition

An Intel RealSense SR300 camera with a resolution of 1920×1080 pixels for the RGB sensor and 640×480 pixels depth sensor was utilized as a 3D scanner to acquire real-world 3D information about the "Venus" and "Belle" objects (295112 and 454972 object points, respectively). The reason why the RealSense camera can be most suitable to the proposed system was that recently mobile devices with the RealSense kit have been started to be manufactured. The non-overlapped EIAs were generated from each point cloud model with a resolution of 1417×1417 pixels using a virtual lens array with 100×100 elemental rectangular lenses (where each lens had a pitch of 1×1 mm and a focal length of 3.3 mm). The original 2D visualizations, point cloud models, and EIAs generated for two objects are shown in Fig. 4.

3.2. SR-based visualization

The SR-based visualization method reconstructs the 3D visualizations of the object with improved resolution and higher-quality. In the experiment, an SR algorithm with a pre-trained CNN model was utilized, because the direct training requires a huge amount of complicated computations; in particular, the quality of some output images may be lower depending on the input images.

Here, first, the orthographic-view image comprised of 14×14 directional-view images were generated from the EIA and stored as separately where the generation time for a single image was approximately 0.0012 s. A super-resolution network for the multiple-degradation (SRMD) model has been chosen as the most suitable SR algorithm for the proposed system because this algorithm satisfied the conditions of the proposed system such as guarantees the most photorealistic quality during the resolution improvement and uncomplicated structure than other similar algorithms [22]. Note that the CNN model could be trained with the initially reconstructed images of the proposed system; however, it would take a long processing time until a model will be trained properly. So, at this time, a pre-trained CNN model has been utilized in the experiment. A CNN model comprised 12 convolutional layers and the feature maps in each layer were set as 128, where the first 11 layers included convolution (for analysis of the image characteristics), a rectified linear unit (activation function of the neural network), and batch normalization layers (for improving the performance and stability of neural networks by adjusting and scaling the input images); the final (12th) layer included only the convolution function (normalization for input images by adjusting and scaling the activations). Here, the kernel of the CNN model used the direct bicubic downsampler, and it was pre-trained in advance from a lot of data sets (images) in sequence with the set degradation maps. Fig. 5 shows the structure of the pre-trained super-resolution network for the multiple-degradation method. The input directional-view images were converted into resolution-enhanced images through the layers of the CNN model and outputted after noise is removed. Note that the computation time of SRMD model for single directional-view image was approximately 0.33 s.

Fig. 6 and Video 1 & 2 present the resolution-enhanced and noise-filtered directional-view images for both objects visualized by a proposed system. We considered the scale factors of $n = 2$ and $n = 4$ and the resolution of the displayed directional-view images was 202×202 pixels ($n = 2$) or 404×404 pixels ($n = 4$), where the resolution of the initial directional-view images was 101×101 pixels.

A total of 11 depth-slices were reconstructed in a 7.5–12.5 mm area at intervals of 0.5 mm (matched according to the normalized depth information) where a single image was generated within 5.43 s. When the scale factor of the SRMD model was $n = 2$, the resolution of each depth slice was 2864×2864 pixels; for the scale factor $n = 4$, the resolution was 5728×5728 pixels, where the original resolution of each depth slice was 1432×1432 pixels and computation time was approximately 5.43 s for single depth-slide. Fig. 7 and Video 3 & 4 show examples of the initially reconstructed depth slices, and images output using an SR-based visualization method. Note that in the actual application environment, it seems better to exclude $n = 4$ case, due to the very large size of the depth-slices.

3.3. Quantitative evaluations

Next, we evaluated the quality of the displayed images and compared the evaluation results with the existing methods. Note that we selected the most suitable SR algorithm for the proposed system through pre-testing among several SR algorithms; therefore, we compared the evaluation results with conventional 3D mobile display [14] and previous interpolation-based resolution enhancing method for it [15], instead of comparing other SR algorithm-based results. Fig. 8 shows the difference in the appearance of the displayed directional-view images derived using the proposed system versus the original 3D mobile system and previous resolution enhancing method for both objects. Here, in order to compare the proposed and previous methods, the interpolation process was executed 1-time (similar to $n = 2$ in the proposed system) and 2-times (similar to $n = 4$ in the proposed system).

As shown in Fig. 8, the images derived using the proposed system were observed much clearer than the other images. Here, when the interpolation process was completed 1-time, the resolution of the input image was improved by a factor of approximately two in each direction, and by almost a factor of four after 2-times of interpolation processes. Furthermore, when the interpolation process was repeated, a decrease in pixel number was observed when using the previous method (201×201 pixels for 1-time of interpolation and 401×401 pixels for 2-times of interpolation), whereas the proposed method multiplied the pixels perfectly.

Similar differences were seen when the depth slices were compared. As shown in Fig. 9, the depth-slices derived using the proposed SR-based method were clearer than the previous interpolation-derived and initially reconstructed images.

Although the proposed system reproduced the clearer resolution-enhanced images, we assessed the differences in quality using the

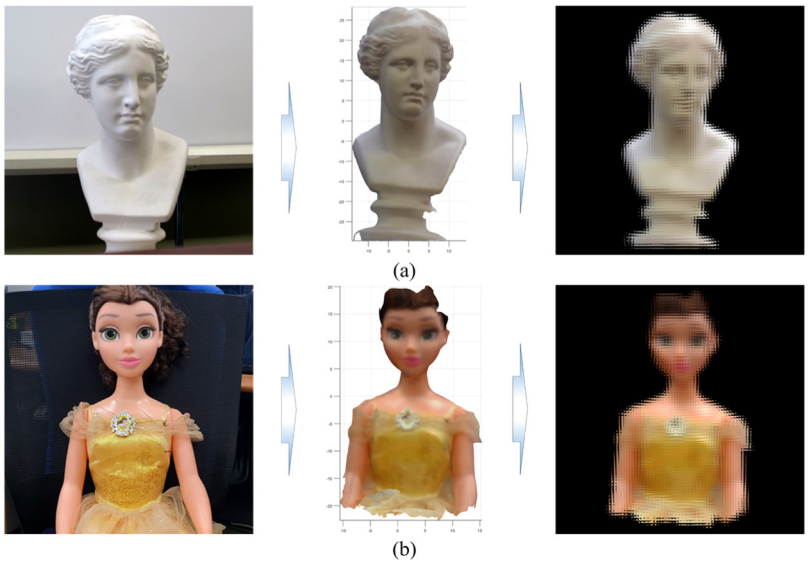

Fig. 4. Original view (left), point cloud models (center) and non-overlapped EIAs generated (right) for the real-world objects (a) Venus and (b) Belle.

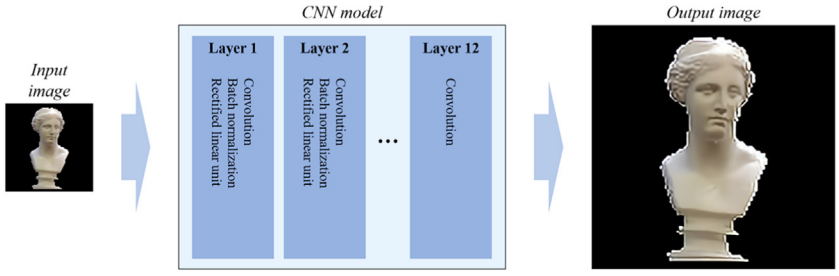

Fig. 5. Schematic diagram of the pre-trained SR model for resolution-enhancement and noise-filtering from the input initially reconstructed images.

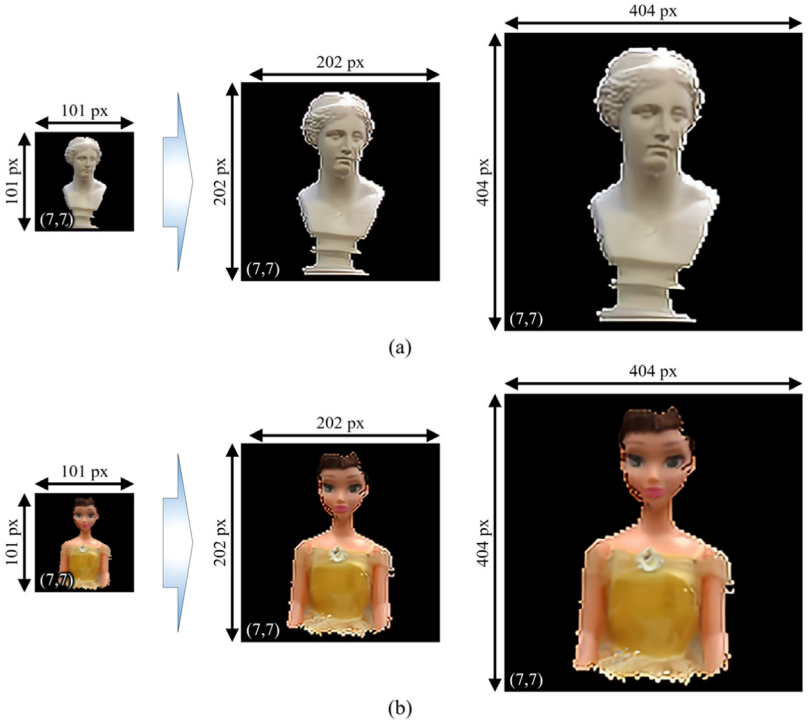

Fig. 6. Examples of original directional-view images (left) and the final output images through the proposed system (center: $n = 2$; right: $n = 4$) for the objects (a) Venus and (b) Belle. Video 1 and Video 2 show the visualizations displayed by a proposed system on the mobile device.

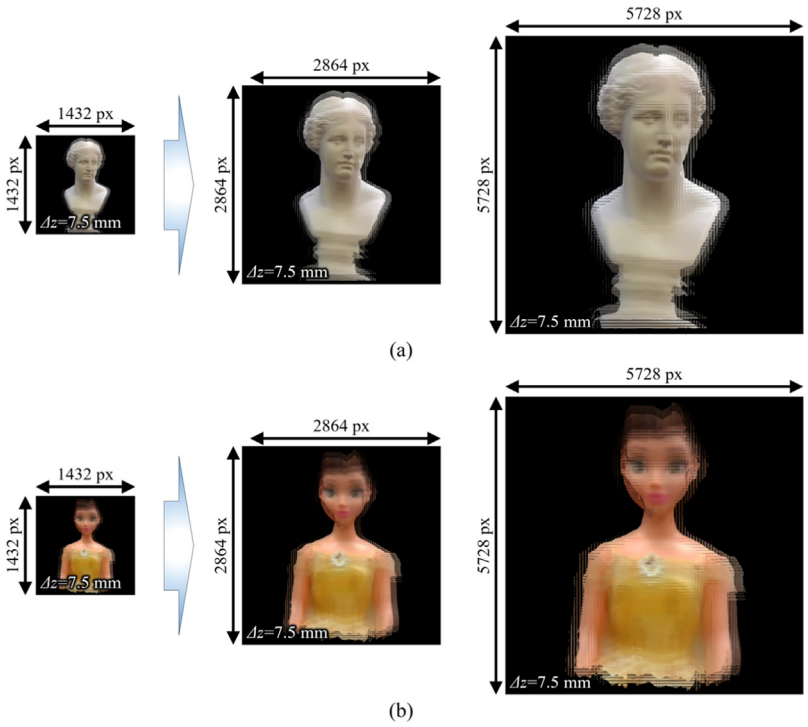

Fig. 7. Examples of initially reconstructed depth-slices (left) and the final output images through the proposed system (center: $n = 2$; right: $n = 4$) for the objects (a) Venus and (b) Belle. Video 3 and Video 4 show the visualizations displayed by a proposed system on the mobile device.

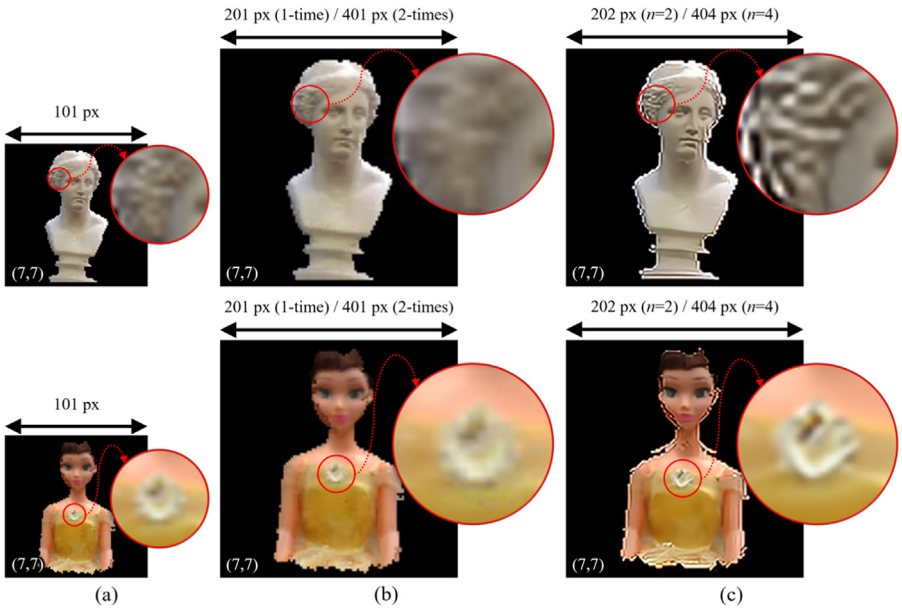

Fig. 8. Comparison of the directional-view images of (a) the initial reconstructions and derived using (b) previous interpolation-based and (c) proposed SR-based methods of both objects.

quantitative measurements. Note that in the experiment, it was difficult to use the reference-based image quality evaluation method such as the peak signal-to-noise ratio; therefore, the reference-free image quality evaluating method for the reconstructed images should be required. In the experiment, the perception-based image quality evaluator (PIQE) and power spectral density (PSD) methods were utilized in order to accurately evaluate the quality of the reconstructed images. The PIQE and PSD values of the reconstructed images of both objects were obtained for the directional-view images with the index (7,7), and for the depth slices with the index $\Delta z = 7.5$ mm and presented in Figs. 10 & 11. In the measurements, the reconstructed images obtained through the previous interpolation-based (1-time and 2-times of interpolation) and proposed (the cases $n = 2$ and $n = 4$) methods have been utilized. Here, the quality of the 2D images of objects and the initially reconstructed images were also evaluated, in order to compare the quality of reconstructed images with the original images.

Figs. 10(a) and 10(b) show the PIQE scores of the displayed directional-view images and depth-slices of Venus and Figs. 10(c) and 10(d) show the PIQE scores of reconstructed images for Belle. In the graphs, "2D" indicates the original 2D images of the objects, "initial" indicates the initially reconstructed images (conventional 3D mobile system), "×2" indicates the cases 1-time of interpolation and n =

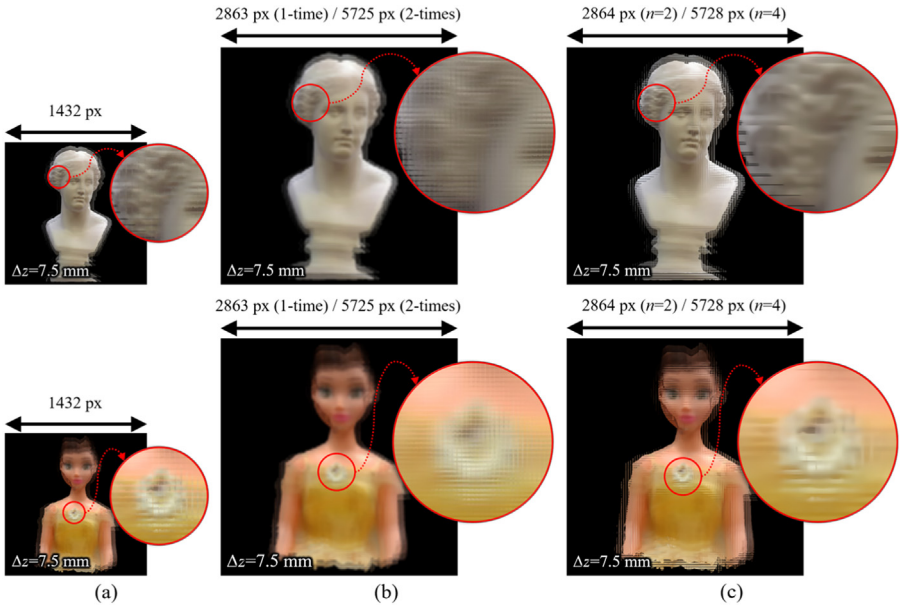

Fig. 9. Comparison of the depth-slices of (a) the original reconstructions, derived using (b) the previous and (c) proposed methods for both objects.

2 for the proposed system, and "×4" indicates the cases 2-times of interpolation and $n = 4$ for the proposed system. For the accurate comparison, the resolution of all images was downscaled to the lowest resolution image. The PIQE scores corresponded to the results of the proposed system (pink) were all less than 70 points, and the scores corresponded to the existing method (blue), 2D image (black) and the initially reconstructed images (gray) were all higher than the proposed system. Note that in the case of PIQE, the lower score determines the better quality.

Fig. 11 shows the PSD values for the corresponding displayed images, 2D images, and initially reconstructed images for both objects. Here, the images were also downscaled to the lowest resolution images (the initially reconstructed directional-view images and depth-slices) in each case of PSD measurement. The PSD values for the displayed images of the proposed system were all higher than 6 dB that similar to the 2D images, where all values were less than 6 dB for the previous method's reconstructions. Note that in the case of PSD, the higher score determines the better quality.

From the above quantitative evaluations, it has been confirmed that the proposed method could reproduce the resolution-enhanced images without a loss in quality under both scale factors; however, compared to the original 2D appearance of the objects, the proposed system still had some quality differences when the initially reconstructed low-quality images were input into the CNN model.

4. Conclusion

A 3D mobile system with deep learning-based advanced visualization method is proposed. A 3D scanner acquires more accurate 3D data for a real object, and the EIA is generated based on the acquired data. From the EIA, the SR-based visualization method reconstructs 3D visualizations of the object with improved resolution while filtering the noise, and the output images displayed on a mobile device. Note that in the proposed system, the computer-generated integral imaging technique is utilized for 3D image processing in order to display the 3D representations of the real object properly on the mobile display; and the lens array-free advanced visualization method reproduces the 3D images in order to utilize the touchscreen of modern smart mobile devices. Also, in the experiment, the pre-trained SRMD algorithm has been utilized as a post-processing CNN-based SR algorithm of the advanced visualization method. Since the 2D mobile display and SR algorithm that does not include the function for estimating the disparity between perspectives are utilized in the proposed system, the analysis for spatial-angular redundancies is not required. The superiority of the displayed images was confirmed visually during the experiment, and the PIQE and PSD measurements confirmed that the proposed system can produce higher-quality images with enhanced resolution, compared to the initially reconstructed images and the previous interpolation method-based outputs. Although we considered only $n = 2$ or $n = 4$ cases in experiments, we proved the possibility of using CNN-based SR methods in 3D mobile systems to display the resolution-enhanced images without compromising quality. The pre-processing, EIA generation, digital reconstruction, and SR-based reconstruction processes were executed using cloud computing due to the performance limitations associated with the mobile environment; therefore, the proposed system is expected to operate efficiently in the mobile devices equipped with RealSense kit with 5G network environment, because of the capacity for transmission of large amounts of data. Further research will consider the acceleration for the image rendering and transmitting processes, and the real-time display within the real low-band 5G network environment with 3.5 GHz frequency. The optical reconstruction using the overlapped EIAs (the size of a single elemental image is set to be larger than each elemental lens) also will be analyzed in further research.

Declaration of competing interest

The authors declare that they have no known competing financial interests or personal relationships that could have appeared to influence the work reported in this paper.

Acknowledgments

This work was supported under the ITRC (Information Technology Research Center) support program (IITP-2020-2015-0-00448 & IITP-2020-0-01846) supervised by the IITP (Institute for Information & communications Technology Promotion), and the National Research Foundation of Korea (NRF) (NRF-2018R1D1A3B07044041), grant funded by the Korea Government.

Appendix A. Supplementary data

Supplementary material related to this article can be found online at https://doi.org/10.1016/j.optcom.2020.126494.

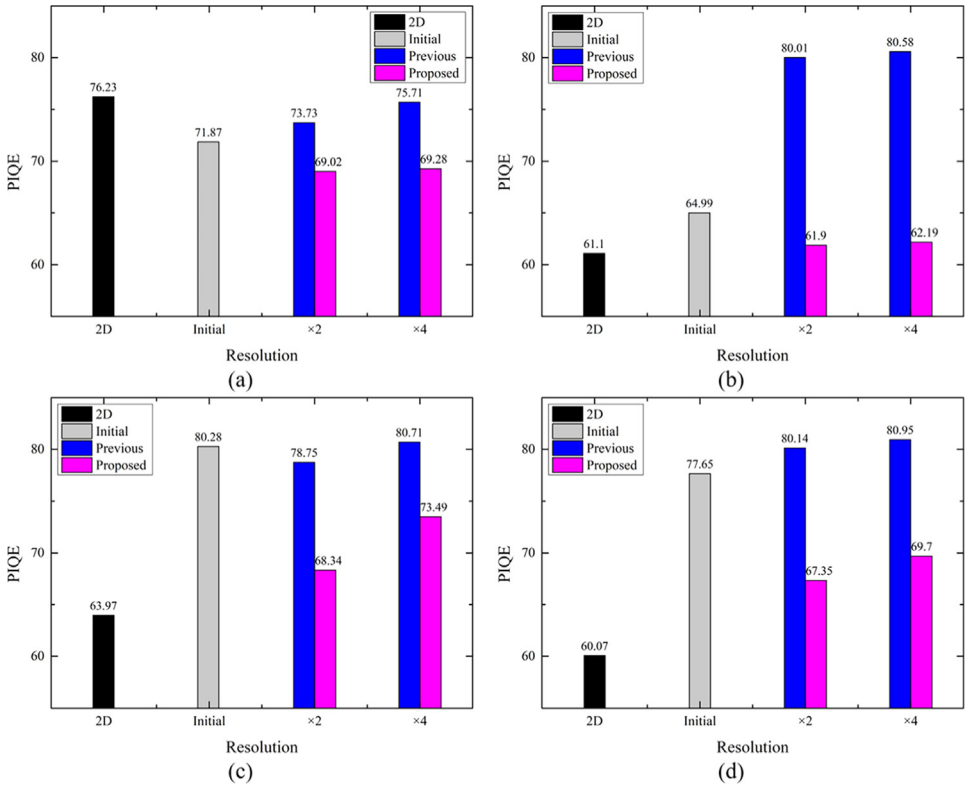

Fig. 10. The PIQE scores of (a) the reconstructed directional-view images and (b) depth slices for Venus; and (c) the directional-view images and (d) depth-slices for Belle.

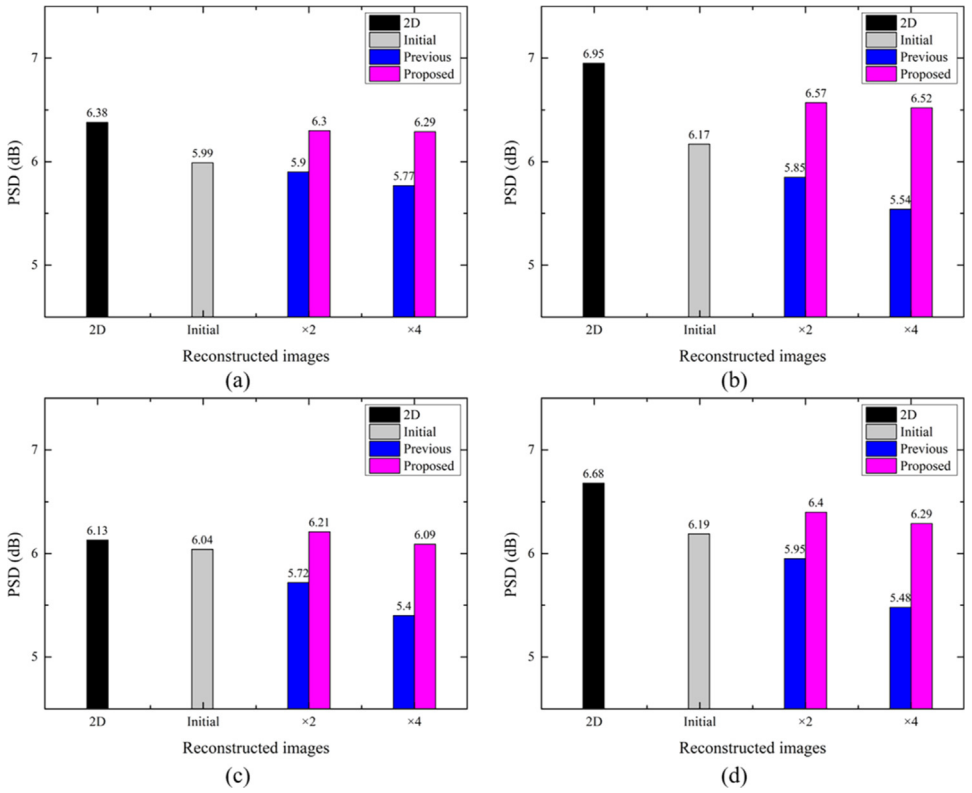

Fig. 11. The PSD values measured from (a) the reconstructed directional-view images and (b) depth slices for Venus; and (c) the directional-view images and (d) depth-slices for Belle, comparing with the corresponding 2D images and initially reconstructed images.

References

[1] M.-U. Erdenebat, Y.-T. Lim, K.-C. Kwon, N. Darkhanbaatar, N. Kim, Waveguide-Type Head-Mounted Display System for AR Application, IntechOpen, 2018, Chap. 4.

[2] N. Kim, M.-U. Erdenebat, 3D Integral Photography, SPIE Press, 2016.

[3] N. Kim, A.-H. Phan, M.-U. Erdenebat, M.A. Alam, K.-C. Kwon, M.-L. Piao, J.-H. Lee, 3D Display technology, Disp. Imag. 1 (1) (2014) 73–95.

[4] N. Kim, M.A. Alam, L.T. Bang, A.-H. Phan, M.-L. Piao, M.-U. Erdenebat, Advances in the light field displays based on integral imaging and holographic techniques, Chin. Opt. Express 12 (6) (2014) 060005.

[5] K.-C. Kwon, C.Y. Im, K.Y. Seo, S.M. Nam, M.-U. Erdenebat, Y.B. Shim, Y.-G. Han, N. Kim, Three-dimensional visualization system for ophthalmic microscopes using visible light and near-infrared illumination, J. Biophotonics 11 (2) (2018) 1–10.

[6] S. Kazempourradi, E. Ulusoy, H. Urey, Full-color computational holographic near-eye display, J. Inf. Disp. 20 (2) (2018) 45–59.

[7] Y. Igarashi, H. Murata, M. Ueda, 3D Display system using a computer generated integral photography, Japan. J. Appl. Phys. 17 (9) (1978) 1683–1684.

[8] S.-W. Min, J. Kim, B. Lee, New characteristic equation of three-dimensional integral imaging system and its applications, Japan. J. Appl. Phys. 44 (2) (2005) 71–74.

[9] G. Li, K.-C. Kwon, G.-H. Shin, J.-S. Jeong, K.-H. Yoo, N. Kim, Simplified integral imaging pickup method for real objects using a depth camera, J. Opt. Soc. Korea 16 (4) (2012) 381–385.

[10] K.-C. Kwon, C. Park, M.-U. Erdenebat, J.-S. Jeong, J.-H. Choi, N. Kim, J.-H. Park, Y.-T. Lim, K.-H. Yoo, High speed image space parallel processing for computer-generated integral imaging system, Opt. Express 20 (2) (2012) 732–740.

[11] D.-H. Kim, M.-U. Erdenebat, K.-C. Kwon, J.-S. Jeong, J.-W. Lee, K.-A. Kim, N. Kim, K.-H. Yoo, Real-time 3D display system based on computer-generated integral imaging technique using enhanced ISPP for hexagonal lens array, Appl. Opt. 52 (34) (2013) 8411–8418.

[12] K.-C. Kwon, J.-S. Jeong, M.-U. Erdenebat, Y.-T. Lim, K.-H. Yoo, N. Kim, Real-time interactive display for integral imaging microscopy, Appl. Opt. 53 (20) (2014) 4450–4459.

[13] J.-S. Jeong, K.-C. Kwon, M.-U. Erdenebat, Y. Piao, N. Kim, K.-H. Yoo, Development of a real-time integral imaging display system based on graphics processing unit parallel processing using a depth camera, Opt. Eng. 53 (1) (2014) 015103.

[14] M.-U. Erdenebat, B.-J. Kim, Y.-L. Piao, S.-Y. Park, K.-C. Kwon, M.-L. Piao, K.-H. Yoo, N. Kim, Three-dimensional image acquisition and reconstruction system on a mobile device based on computer-generated integral imaging, Appl. Opt. 56 (28) (2017) 7796–7802.

[15] M.-U. Erdenebat, Y.-L. Piao, N. Darkhanbaatar, K.-C. Kwon, N. Kim, Advanced mobile three-dimensional display based on computer-generated integral imaging, Proc. SPIE 10679 (2018) 106790I.

[16] K.-C. Kwon, J.-S. Jeong, M.-U. Erdenebat, Y.-L. Piao, K.-H. Yoo, N. Kim, Resolution-enhancement for an orthographic-view image display in an integral imaging microscope system, Biomed. Opt. Express 6 (3) (2015) 736–746.

[17] C. Dong, C.C. Loy, K. He, X. Tang, Image super-resolution using deep convolutional networks, IEEE Trans. Pattern Anal. Mach. Intell. 38 (2) (2015) 295–307.

[18] J. Kim, J.K. Lee, K.M. Lee, Accurate image super-resolution using very deep convolutional networks, in: Proceedings of IEEE Conference on Computer Vision and Pattern Recognition, IEEE, 2016, pp. 1646–1654.

[19] W.-S. Lai, J.-B. Huang, N. Ahuja, M.-H. Yang, Fast and accurate image super-resolution with deep Laplacian pyramid networks, IEEE Trans. Pattern Anal. Mach. Intell. 41 (11) (2018) 2599–2613.

[20] C. Dong, C.C. Loy, X. Tang, Accelerating the super-resolution convolutional neural network, in: Proceedings of European Conference on Computer Vision, Springer, 2016, pp. 391–407.

[21] C. Ledig, L. Theis, F. Huszar, J. Caballero, A. Cunningham, A. Acosta, A. Aitken, A. Tejani, J. Totz, Z. Wang, W. Shi, Photo-realistic single image super-resolution using a generative adversarial network, in: Proceedings of IEEE Conference on Computer Vision and Pattern Recognition, IEEE, 2017, pp. 4681–4690.

[22] K. Zhang, W. Zuo, L. Zhang, Learning a single convolutional super-resolution network for multiple degradations, in: Proceedings of IEEE Conference on Computer Vision and Pattern Recognition, IEEE, 2018, pp. 3262–3271.

[23] K.-C. Kwon, K.H. Kwon, M.-U. Erdenebat, Y.-L. Piao, Y.-T. Lim, M.Y. Kim, N. Kim, Resolution-enhancement for an integral imaging microscopy using deep learning, IEEE Photon. J. 11 (1) (2019) 6900512.

[24] H. Ren, Q.-H. Wang, Y. Xing, M. Zhao, L. Luo, H. Deng, Super-multiview integral imaging scheme based on sparse camera array and CNN super-resolution, Appl. Opt. 58 (5) (2019) A190–A196.

[25] Y. Li, X. Sang, S. Xing, Y. Guan, S. Yang, D. Chen, L. Yang, B. Yan, Real-time optical 3D reconstruction based on Monte Carlo integration and recurrent CNNs denoising with the 3D light field display, Opt. Express 27 (16) (2019) 22198–22208.

[26] Y. Ko, S. Yi, Development of color 3D scanner using laser structured-light imaging method, Curr. Opt. Photon. 2 (6) (2018) 554–562.

[27] S. Katz, A. Tal, R. Basri, Direct visibility of point sets, ACM Trans. Graph. 26 (3) (2007) 24.

[28] M.-U. Erdenebat, K.-C. Kwon, E. Dashdavaa, Y.-L. Piao, K.-H. Yoo, G. Baasantseren, Y. Kim, N. Kim, Advanced 360-degree integral-floating display using a hidden point removal operator and a hexagonal lens array, J. Opt. Soc. Korea 18 (6) (2014) 706–713.

[29] A. Said, E.-V. Talvala, Spatial-angular analysis of displays for reproduction of light fields, Proc. SPIE 7237 (2009) 723707.

[30] A. Ivan, I.K. Park, Joint light field spatial and angular super-resolution from a single image, IEEE Access 8 (2020) 112562–112573.

[31] ITFIND, Weekly technology trend, 1894, http://www.itfind.or.kr/publication/regular/weeklytrend/weekly/list.do?selectedId=1076.